BioOne COMPLETE

Adsorption of Acid Blue 25 on Agricultural Wastes: Efficiency, Kinetics, Mechanism, and Regeneration

Authors: Samat, Junaidi H, Shahri, Nurulizzatul Ningsheh M, Abdullah, Muhammad Ashrul, Suhaimi, Nurul Amanina A, Padmosoedarso, Kanya Maharani, et al.

Adsorption of Acid Blue 25 on Agricultural Wastes: Efficiency, Kinetics, Mechanism, and Regeneration

Junaidi H Samat[1], Nurulizzatul Ningsheh M Shahri[1], Muhammad Ashrul Abdullah[1], Nurul Amanina A Suhaimi[1], Kanya Maharani Padmosoedarso[2], Eny Kusrini[2], Abdul Hanif Mahadi[1], Jonathan Hobley[3] and Anwar Usman[1] (iD)

[1]Universiti Brunei Darussalam, Gadong, Brunei Darussalam. [2]Universitas Indonesia, Depok, Indonesia. [3]National Cheng Kung University, Tainan City, Taiwan.

ABSTRACT: In this study, Acid Blue 25 (AB25), which is a negatively charged synthetic dye was removed from an aqueous solution by adsorption onto agricultural wastes, including banana (BP) and durian (DP) peels. The adsorption performances of AB25 were related to surface characteristics of the agricultural wastes, including their chemical functional groups, net surface charge, surface morphology, surface area, and pore volume. Parameters affecting the adsorption, including contact times, initial concentration, pH, and temperature were investigated. The results revealed that the adsorption of AB25 followed pseudo-second order kinetics, and that the adsorption process was controlled by a combination of intraparticle and film diffusion with a two-step mechanism. The equilibrium data could be simulated by the Langmuir isotherm model, suggesting that AB25 molecules are adsorbed on active sites with a uniform binding energy as a monolayer on the adsorbent surface. The adsorption process was spontaneous and exothermic, and the adsorption capacity decreased with the pH of the medium. The spent adsorbents were best regenerated by acid treatment (pH 2), and could be recycled for several adsorption-desorption processes. Under ambient conditions, the maximum adsorption capacities of AB25 on BP and DP were 70.0 and 89.7 mg g^{-1}, respectively, which is much higher than on a large variety of reported adsorbents derived from other agricultural wastes.

KEYWORDS: Adsorption, acid blue 25, banana peel, durian peel, agricultural wastes

Introduction

The massive scale of industrialization has delivered major technological advances to the current modern world. As a consequence, many short-term benefits have been claimed at the expense of long-term environmental damage to the air, soil, and water. In particular, water systems are contaminated by effluents containing heavy metals, synthetic chemicals, and byproducts, which are known to be toxic, mutagenic, carcinogenic, or teratogenic to various microorganisms and humans (Boretti & Rosa, 2019). The preemptive solution to this problem is to remove these pollutants from industrial wastewater before discharging it into water systems (Palani et al., 2021). Among most promising practical methods to achieve this, adsorption has received a great attention due to its simplicity and applicability (Piaskowski et al., 2018; Rafatullah et al., 2010). To date a wide range of materials, such as activated carbons (Alwi et al., 2020; Srivatsav et al., 2020), natural clays (Alshameri et al., 2019), zeolite-based composites (Zamri et al., 2021), and agricultural wastes (Zaidi et al., 2019) have been utilized as adsorbents. In particular, agricultural wastes have several obvious advantages, including their availability in large quantity at low cost, and because their surfaces contain a variety of functional groups (De Gisi et al., 2016).

One of the synthetic dyes commonly utilized in industries and found in effluents is the negatively charged Acid Blue 25 (AB25) (Lewis, 2009). Because of this, the adsorptive removal of AB25 from an aqueous solution has been studied as a model for treatment of wastewater contaminated by acidic synthetic dyes. It has been investigated by employing various types of adsorbent, including activated carbons (Auta & Hameed, 2011; Tovar-Gómez et al., 2012), plants (Kousha et al., 2014), agricultural wastes such as cempedak durian peel (Dahri et al., 2016), pine sawdust (Ferrero, 2007), oak sawdust (Ferrero, 2007), peach seed (Kul et al., 2019), hazelnut shells (Ferrero, 2007), *Ficus rasemosa* powdered leaves (Jain & Gogate, 2017), *Azolla pinnata* (Kooh et al., 2016), soybean waste (Kooh et al., 2016), walnut sawdust (Ferrero, 2007), powdered rubber leaves (Khalid et al., 2015), *Shorea dasyphylla* sawdust (Hanafiah et al., 2012), rambutan seed (Lakkaboyana et al., 2018), prawn shells (Kousha et al., 2015), polymer-clay nanocomposites (El-Hamshary et al., 2020), and pectin (Shahrin et al., 2021). With this library of data, it is now possible to begin to relate the adsorption behavior of AB25 to the specific surface characteristics of each agricultural waste. Several functional surface groups are present on various agricultural wastes, that are relevant in their adsorption characteristics. For example, there can be carboxylic acid (–COOH), hydroxyl (–OH), carbonyl (–C=O), amine (–NH$_2$), and ester (–O–) groups. In the case of carboxylic acid bound to alkyl and aromatic compounds, the typical pKa is in the range of 3.4 to 4.8 (Zeng et al., 2012). Therefore, at ambient pH, agricultural wastes with carboxylic acid groups, would have a negative net surface charge which could suppress their electrostatic attraction to the negatively charged dyes. This assumption is supported by the low adsorption capacity of AB25, for instance, on cempedak durian peel (Dahri

et al., 2016), pine sawdust (Ferrero, 2007), peach seed (Kul et al., 2019), powdered *Ficus rasemosa* leaves (Jain & Gogate, 2017), *Azolla pinnata* (Kooh et al., 2016), soybean waste (Kooh et al., 2016), and rambutan seed (Lakkaboyana et al., 2018). This explanation could also apply to other negatively charged dyes such as Acid Green 25 (AG25) on durian peel (DP) (Hameed & Hakimi, 2008), Acid Violet 54 (AV54) on banana peel (BP) (Kumar et al., 2010), Congo red (CR) on BP (Mondal & Kar, 2018), and Acid violet 17 (AV17) on orange peel (Chiou & Chuang, 2006). To further test this assumption, in this study, the adsorptive removal of AB25 on BP and DP was investigated and compared with those reported other agricultural wastes. BP and DP were selected as these two agricultural wastes have been successfully applied as adsorbents for the removal of synthetic dyes (Asbollah et al., 2021; Guiso et al., 2014; Hameed & Hakimi, 2008; Jawad et al., 2018; Mohammed et al., 2012; Mondal & Kar, 2018), physical pollutant (Payus et al., 2021), and heavy metals (Deshmukh et al., 2017). Therefore, the objective of this current study is to evaluate adsorptive removal of AB25 on BP and DP in a batch system and to establish the relevant functional groups, the pH of zero charge (pH_{pzc}), the surface morphology, and surface characteristics of the adsorbents. We aim to relate these to the adsorption behavior of AB25. The kinetics, isotherm, mechanism, maximum capacity, and thermodynamics of the adsorption of AB25 onto BP and DP were analyzed in detail based on the effects of contact time, initial concentration, pH, and temperature. The maximum monolayer adsorption capacity (Q_m) values of AB25 on BP and DP were compared with those on other reported adsorbents derived from a variety of agricultural wastes. Finally, desorption of AB25 from the spent BP and DP were also investigated by washing them in acidic, basic, and aqueous solutions, and the regenerated adsorbents were reapplied for the removal of AB25.

Materials and Methods

Preparation of sorbents

Both banana (*Musa paradisiaca* L.) and durian (*Durio zibethinus* M.) were obtained from a local market in Brunei. The fruits were peeled, and the peels were chopped into small pieces (less than 2×2 cm). They were then put in aluminum trays and dried in an oven at 40°C. After drying, they were ground into a coarse powder using a blender (Zojirushi Mill BM-RT08-GA), then sieved through a 212-μm stainless steel metal mesh to ensure that that the BP and DP have a similar particle size distribution. To prevent atmospheric water adsorption, both adsorbents were kept in sealed plastic bags before use.

Characterization of adsorbents

The functional surface groups of BP and DP were identified based on their vibrational spectra obtained using an FTIR Prestige-21 spectrometer (Shimadzu). The spectra were recorded using the KBR pellet technique over the full frequency range of the spectrometer (4000–400 cm⁻¹) to test for the presence of all possible organic functional groups on the adsorbent surface. The surface morphology of the adsorbents was assessed by SEM imaging on a JSM-7600F microscope (JEOL) operating at 5.0 kV. Their Brunauer–Emmett–Teller (BET) surface area and Barrett-Joyner-Halenda (BJH) pore volume were determined based on multipoint adsorption-desorption of nitrogen gas using an ASAP 2020 V4.02 surface analyzer (Micromeritics). The adsorption and desorption isotherms were carried out at 77.4 K. The process included degassing and adsorption of N_2 from 10^{-5} atm to atmospheric pressure. Finally, in order to observe the desorption isotherm process, the pressure was reduced from atmospheric pressure to high vacuum. The surface charge of the adsorbents was characterized by monitoring the change in pH of 20 mL (0.1 mol L⁻¹) KNO_3 solutions containing 200 mg adsorbent. The initial pH of the KNO_3 solutions was adjusted to be in the range of 2 to 12 by adding HCl or NaOH, and their final pH was measured after shaking the suspensions for 24 hours.

AB25 adsorption

AB25 (1-amino-4-anilino-9,10-dioxoanthracene-2-sulfonate sodium salt; $C_{20}H_{13}N_2NaO_5S$; CAS# 6408-78-2; MW 416.38 g mol⁻¹) was purchased from Sigma-Aldrich Co. Various concentrations of AB25 in distilled water were prepared by successive dilution of its 1 g L⁻¹ stock solution. Prior to adsorption experiments, absorption spectra of the prepared AB25 solutions were measured in the spectral range of 200 to 800 nm in a 1 cm quartz cuvette cell using a UV-visible spectrophotometer (UV-1900, Shimadzu).

The adsorption of AB25 on BP and DP was carried out using the batch method; where 100 mg of the adsorbents was suspended in 10 mL AB25 solutions (2.40×10^{-4} mol L⁻¹) in several conical flasks. The suspensions were shaken using an orbital water bath shaker at 100 rpm. After a desired contact time, the adsorption process was terminated, the mixture was vacuum filtered through a filter paper, and absorption spectrum of the supernatant was measured. The initial concentration (C_0) and remaining concentration (C_t) of AB25 in the solution were accurately determined using the Beer-Lambert law based on the molar extinction coefficient of the synthetic dye at 600 nm being 1.05×10^4 L mol⁻¹ cm⁻¹ (Guiso et al., 2014). The experimental conditions were then carefully controlled, and the effects of contact time (0–240 minutes), initial AB25 concentration (0.24×10^{-4}–4.80×10^{-4} mol L⁻¹), the pH of the medium (pH 3–10) and its temperature (20°C–45°C) were systematically evaluated. In addition, the spent adsorbents were collected and dried for SEM and FTIR analyses.

Adsorption kinetics and isotherm

Based on the C_0 and C_t values of AB25, the adsorption capacity (Q_t) of the synthetic dye at different contact times was then calculated as;

$$Q_t = \frac{(C_0 - C_t)}{M} \times V \qquad (1)$$

Here, M is the mass of BP or DP in the suspensions, and V is the volume of AB25 solution. The adsorption kinetics were established by simulating the Q_t values with linear equations of the Lagergren pseudo-first order (Simonin, 2016) and pseudo-second order models (Robati, 2013), as given by

$$\ln(Q_e - Q_t) = \ln Q_e - k_1 t \qquad (2)$$

$$t/Q_t = 1/k_2 Q_e^2 + t/Q_e \qquad (3)$$

where k_1 and k_2 are the rate constants of the pseudo-first order and pseudo-second order kinetics, respectively, and Q_e is the adsorption capacity at equilibrium. In order to evaluate the diffusion mechanism and mass transfer processes, including intraparticle and film diffusions of AB25 onto BP and DP, the same Q_t data were simulated by the Weber–Morris intraparticle (Ho et al., 2000) and the Boyd diffusion models (Viegas et al., 2014) using;

$$Q_t = k_i t^{1/2} + C \qquad (4)$$

$$B_t = -0.4977 - \ln(1 - Q_t/Q_e) \qquad (5)$$

where k_i represents the rate constant of intraparticle diffusion, C is the thickness of the boundary layer, and B_t is the Boyd constant.

In order to gain insight into the adsorption mechanism and the distribution of AB25 molecules adsorbed on the BP and DP surfaces, the Q_e values obtained at different initial AB25 concentrations were simulated using linear equations of the Langmuir (equation (6)), Freundlich (equation (7)), Temkin (equation (8)), and Dubinin-Radushkevich (equation (9)) isotherm models (Ghaffari et al., 2017), as given by

$$1/Q_e = 1/Q_m K_L \times 1/C_e + 1/Q_m \qquad (6)$$

$$\log Q_e = 1/n \times \log C_e + \log K_F \qquad (7)$$

$$Q_e = \frac{RT}{b_t}(\ln K_T + \ln C_e) \qquad (8)$$

$$\ln Q_e = \ln Q_m - \beta\left\{RT\ln(1/C_e)\right\}^2 \qquad (9)$$

where, K_L and K_F are the Langmuir and Freundlich isotherm constants, n is the Freundlich exponent, K_T and b_t are the Temkin isotherm constants, β is the change in the Dubinin-Radushkevich mean free energy, R is the gas constant, and T is temperature.

The effect of temperature

The thermodynamics of the adsorption process were established based on the effect of temperature on the equilibrium. In this sense, the K_L values obtained from the adsorption of AB25 at different temperatures were converted into dimensionless equilibrium constant (K_e^0) values (Lima et al., 2019) using

$$K_e^0 = K_L \times [AB25]/\gamma \qquad (10)$$

where $[AB25]$ is the concentration of AB25 solution which was in the order of $10^{-4}\,mol\,L^{-1}$, and the γ value is the activity coefficient which was assumed to be 1 because the solution is dilute.

Adsorbent regeneration

A 100 mL AB25 solution ($2.40 \times 10^{-4}\,mol\,L^{-1}$) containing suspensions of 1 g of BP or DP was shaken for 180 minutes at room temperature to generate adsorbent that is fully loaded with AB25. After filtration, the spent adsorbent was collected and dried. The spent adsorbent was then divided into three equal fractions, and each of them was soaked in different desorbing agents; 50 mL HCl (0.01 M, pH 2), 50 mL NaOH (0.01 M, pH 12), or 50 mL distilled water. These suspensions were then shaken for 120 minutes at room temperature. Next, the suspensions were vacuum filtrated, followed by drying. The regenerated adsorbents were then recycled and again used for the removal of AB25, following the procedures described in the previous Section. The adsorption-desorption process of AB25 was repeated and adsorption performance of the regenerated BP and DP were tested for several cycles.

Results and Discussion

Functional groups of BP and DP

Figure 1 shows the FTIR spectra of BP and DP before and after AB25 adsorption. For reference, the FTIR spectrum of AB25 is also shown. Before adsorption, the FTIR spectra of BP and DP had similar features, where the main bands were observed at 3400, 2922, 2849, 1733, and 1159 cm^{-1} which have been assigned to the stretching vibrations of O–H, N–H, C–H, C=O, and C–O (alcohol) or C–N groups, respectively (Dinh et al., 2019; Jawad et al., 2018; Zaidi et al., 2018). There are several low intensity bands at 1648, 1433, and 1065 cm^{-1} which could be attributed to non-aromatic or unconjugated C=C stretching vibration, C–H bending vibrations, and C–C vibrational modes of conjugated aromatic rings. The spectral bands at 1618 and 1381 cm^{-1} have been assigned to the bending vibrations of aromatic C–H group and carboxylic acid O–H group (Dinh et al., 2019; Jawad et al., 2018; Zaidi et al., 2018).

The FTIR spectra therefore indicate that both BP and DP contain several functional groups with strong hydrogen
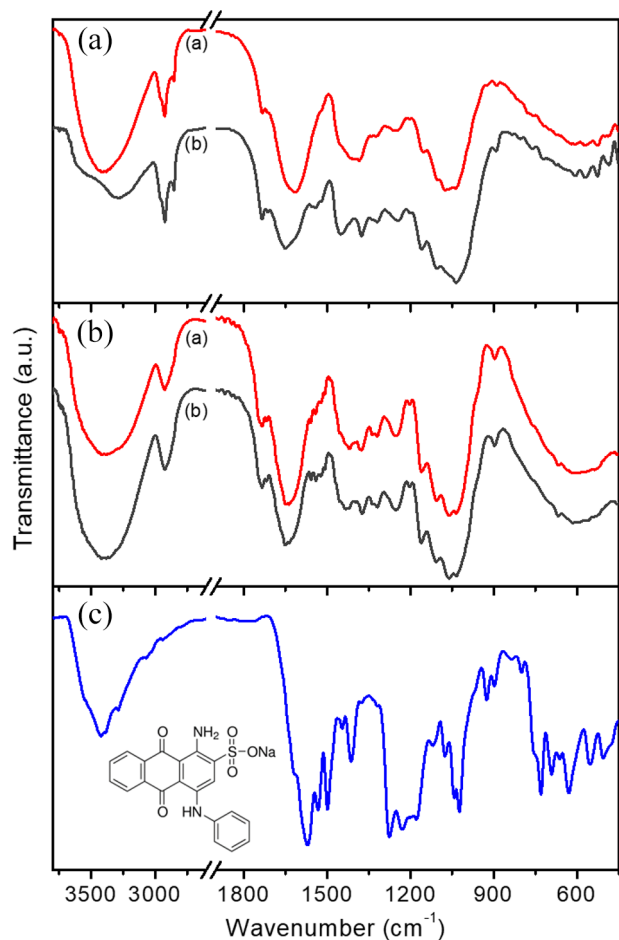
Figure 1. FTIR spectra of: (a) BP and (b) DP before (■) and after (■) AB25 adsorption, and (c) AB25 (Inset: the molecular structure of AB25).

bonding capabilities, such as COOH, OH, C=O, and NH_2 groups. These functional groups on the adsorbent surface can form dipolar and H-bonding interactions with C=O, S=O, and NH_2 groups of AB25, through which should make the adsorption of AB25 on the adsorbent surface very efficient. The similar spectral features of BP and DP suggested that these agricultural wastes contained the same functional groups, meaning that AB25 is probably adsorbed on both adsorbents in the same way.

The FTIR spectra of BP and DP were almost unchanged upon the adsorption of AB25, indicating that functional groups of the adsorbents remained intact. Nevertheless, several new minor peaks around 1200 to 1600 cm^{-1} were clearly observed which could be assigned to either the vibrational bands of AB25 adsorbed on the adsorbent surfaces or the possible peak shift of the adsorbents upon AB25 adsorption. It is also noteworthy that, upon the adsorption of AB25, the OH vibrational band of BP at 3400 cm^{-1} split into two bands at 3282 and 3582 cm^{-1} due most likely to active participation of this functional group in AB25 adsorption. Overall, the FTIR spectra indicate that the negatively charged synthetic dye could easily bind to the adsorbents via hydrogen and dipolar bonding interactions.

Surface morphology and surface charge of BP and DP

SEM images (10,000× magnification) of BP and DP are shown in Figure 2. Due to differences in the roughness of the two adsorbents different working distances (WD) were used in order to control the depth of field so that the full field was imaged without aberration. However, the WD is related to the numerical aperture and therefore the resolution of the image. Therefore, for SEM images recorded at different WDs in the range of 0.1 to 0.6 mm (see Figure 2), the pore structures on the surface of BP and DP cannot be directly compared. Nevertheless, the SEM images provide the surface morphology before and after dye adsorption, as reflected by the line profile of a horizontal line-scans passing horizontally (*x*-axis) through the center of the images. Since the contrast in these images is obviously following the surface topography the line-scans are taken to indicate surface roughness. From these line-scans it is clearly observed that the surface roughness of BP was reduced after AB25 adsorption while for DP it increased after AB25 adsorption. These changes in the surface morphology were also revealed by their surface characteristics, where the BET surface area and BJH pore volume of BP was reduced whereas that of DP increased, as summarized in Table 1. The plot of N_2 adsorption and desorption isotherms, as shown in Supplemental Figure S1, indicated that BP and DP contained macroporous structure.

The surface charge characteristic of BP and DP was revealed by plotting their ΔpH versus the initial pH of KNO_3 solution, as shown in Supplemental Figure S2. The *x*-intercept of the plots suggested that pH_{pzc} values of BP and DP were 6.32 and 6.18, respectively, which were within the values reported for a variety of agricultural wastes (Pathak et al., 2017). This finding supports the conclusion that the adsorbents derived from agricultural wastes, in general, have similar functional groups. With respect to the pH_{pzc} values, under the ambient experimental conditions (pH 6.7), the BP and DP surfaces will be negatively-charged due to the deprotonation of their carboxylic acid groups.

AB25 adsorption on BP and DP

Although the adsorption capacity of AB25 in the presence of BP and DP should be affected by the pH of the medium, the adsorption kinetics and isotherm of the synthetic dye were evaluated at ambient pH 6.7. Figure 3 shows the absorption spectra of AB25 solution at different contact times from 0 to 240 minutes. The decrease in absorption intensity resulted from the adsorption of AB25, as demonstrated by the time dependence of Q_t values in Supplemental Figure S3. It is clearly observed that the adsorption capacities of AB25 on BP and DP increased with contact time and saturated at contact times longer than 150 minutes. At equilibrium, the Q_e values of AB25 on BP and DP were 4.07 and 4.49 $mg\,g^{-1}$, respectively. Figure 4(a) and (b) show the adsorption kinetic data, represented by the Q_t values, simulated using the Lagergren
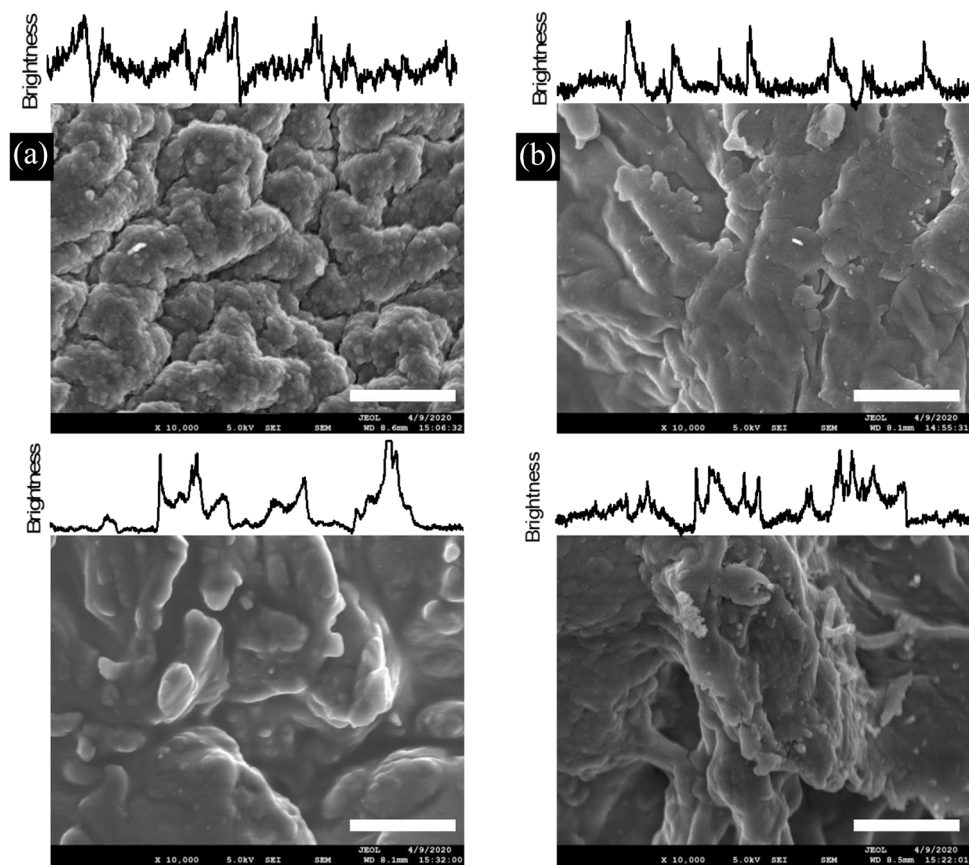
Figure 2. SEM images of (a) BP and (b) DP before (top row) and after AB25 adsorption (bottom row). All images were recorded at the same magnification (10,000×). The scale bars represent 3 μm. The line profiles on top of each image represent horizontal line scans from edge to edge passing through the center of the image.

Table 1. The BET Surface Area and Pore Size of BP and DP Before and After AB25 Adsorption.

ADSORBENT	BEFORE ADSORPTION		AFTER ADSORPTION	
	BET SURFACE AREA ($M^2 G^{-1}$)	PORE VOLUME ($CM^3 G^{-1}$)	BET SURFACE AREA ($M^2 G^{-1}$)	PORE VOLUME ($CM^3 G^{-1}$)
BP	0.321	0.119	0.2135	0.064
DP	0.703	0.213	3.235	0.464

pseudo-first order and pseudo-second order kinetic models. As summarized in Table 2, the regression coefficient (R^2) values of the two kinetics model were 0.519 and 0.999 for the adsorption of AB25 on BP, and they were 0.627 and 0.999 for the adsorption of AB25 on DP. These results suggest that adsorption kinetics of AB25 on both adsorbents was pseudo-second order with the rate constant of AB25 on BP (0.163 g mg⁻¹ minutes⁻¹) being faster compared to that on DP (0.092 g mg⁻¹ minutes⁻¹). The pseudo-second order kinetics implies that the adsorption of AB25 on BP and DP was controlled by chemical interactions (Hubbe et al., 2019), as was also suggested by the FTIR spectral analyses in the previous section.

Figure 4(c) shows the best simulation of the Weber–Morris intraparticle diffusion model on the adsorption kinetic data. The simulation plots showed two linear trends and one breakpoint, suggesting that the adsorption of AB25 occurred in a two-step intraparticle diffusion process. For BP, at early contact times, a fast intraparticle diffusion was observed with a rate of 0.246 mg g⁻¹ minutes⁻¹/² due to external mass transfer of AB25 onto the BP. This was followed by slower pore-volume diffusion at the equilibrium phase of the reaction with the rate of 0.035 mg g⁻¹. Similarly, a two-step intraparticle diffusion was observed for DP, with the fast and slow diffusion rates being 0.368 and 0.046 mg g⁻¹ minutes⁻¹/².

It is important to note that the intercept of the Weber–Morris plots deviates from the origin, suggesting the existence of boundary layer effect which could hinder the intraparticle diffusion (Fierro et al., 2008) and that the adsorption process was not solely controlled by the intraparticle diffusion (Dotto & Pinto, 2012). This conclusion was further supported by analyzing the adsorption kinetic data using the Boyd diffusion model in Figure 4(d), where the simulation plots revealed two linear
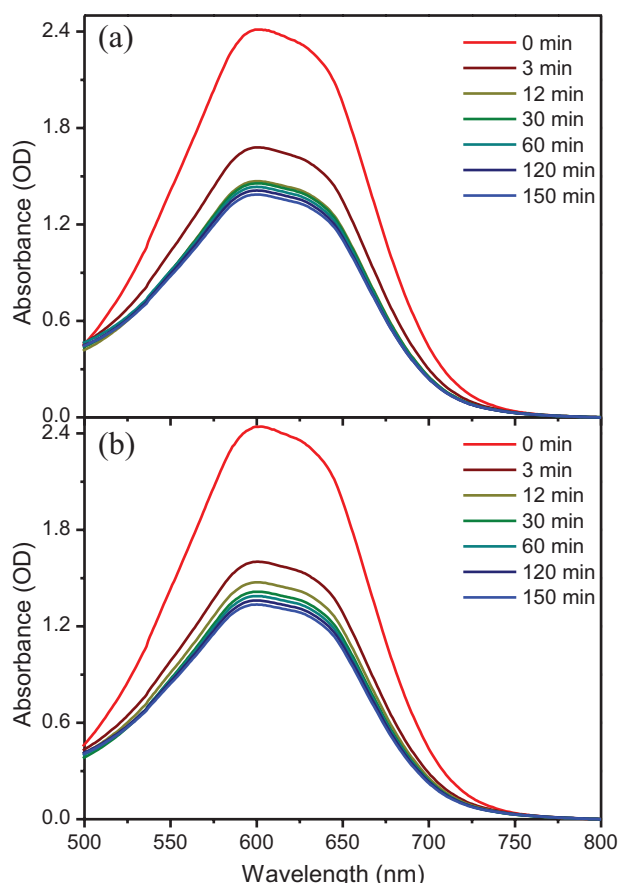
Figure 3. Absorption spectra of 2.40×10^{-4} mol L^{-1} AB25 solutions in the presence of (a) 100 mg of BP and (b) 100 mg of DP at different contact times.

trends with one breakpoint and the intercept of the simulation plots also deviated from the origin. Based on the Boyd diffusion criteria (El-Khaiary & Malash, 2011; Sharma & Das, 2013), these findings indicate that the adsorption of AB25 on BP and DP occurs with a combination of intraparticle and film diffusion mechanisms.

Adsorption isotherms

Figure 5 shows the adsorption isotherms of AB25 on BP and DP simulated using empirical isotherm models. The experimental data points were well simulated by both the Langmuir and Freundlich isotherm models (Figure 5(a) and (b)), whilst they deviated from the simulation plots of the Temkin and Dubinin–Radushkevich isotherm models (Figure 5(c) and (d)). As summarized in Table 3, the linear regression coefficient (R^2) values of the fitting lines confirmed that the adsorption mechanism and distribution of AB25 molecules adsorbed on the BP and DP surfaces followed the Langmuir isotherm model. This suggests that AB25 molecules were adsorbed on active sites with homogeneous binding energy as a single monolayer on the adsorbent surface. Using the Dubinin–Radushkevich mean free energy, the average adsorption energy ($E = (2\beta)^{-1/2}$) was estimated to be in the range of 3.78–3.80 kJ mol^{-1}. The low

magnitude of the binding energy can be attributed to hydrogen bonding interactions dominating the process (Bhatt & Shah, 2015). This further supports the conclusions reached from assignments of the FTIR spectral bands in the previous section. The Langmuir isotherm model estimated the Q_m values of AB25 on BP and DP to be 70.0 and 89.7 mg g^{-1}, respectively.

Comparison of Q_m values for adsorption of AB25 on different adsorbents

As the adsorption behavior of AB25 should depend on the functional groups, surface area, and pore size of the adsorbents, it is interesting to compare the Q_m values of AB25 on different adsorbents. As listed in Table 4, the Q_m values of AB25 on BP and DP were much lower compared to those on modified activated carbon derived from egg shell (109.8 mg g^{-1}) (Tovar-Gómez et al., 2012), lychee peel (200.0 mg g^{-1}) (Bhatnagar & Minocha, 2010), tea waste activated carbon (203.3 mg g^{-1}) (Auta & Hameed, 2011), *Penaeus indicus* shell (415.3 mg g^{-1}) (Kousha et al., 2015), and pectin (719.4 mg g^{-1}) (Shahrin et al., 2021). However, they were comparable or slightly higher with those on several agricultural wastes such as peach seed (95.2 mg g^{-1}) (Kul et al., 2019), modified banana peel (89.5 mg g^{-1}) (Guiso et al., 2014), hazelnut shells (60.2 mg g^{-1}) (Ferrero, 2007), and *Ficus rasemosa* leaf powder (83.3 mg g^{-1}) (Jain & Gogate, 2017), and were much higher than adsorbents derived from other agricultural wastes as such as *Azolla pinnata* (50.5 mg g^{-1}) (Kooh et al., 2016), soybean waste (38.3 mg g^{-1}) (Kooh et al., 2016), walnut sawdust (37.0 mg g^{-1}) (Ferrero, 2007), rubber leaf powder (28.1 mg g^{-1}) (Khalid et al., 2015), *Shorea dasyphylla* sawdust (24.4 mg g^{-1}) (Hanafiah et al., 2012), cempedak durian peel (26.6 mg g^{-1}) (Dahri et al., 2016), pine sawdust (26.2) (Ferrero, 2007), oak sawdust (27.9 mg g^{-1}) (Ferrero, 2007), and rambutan seed (25.6 mg g^{-1}) (Lakkaboyana et al., 2018). These findings indicate that BP and DP were among the best of the potential agricultural wastes to remove negatively charged dyes from an aqueous solution. In addition, it is also interesting to compare the Q_m values of AB25 with those of other acidic synthetic dyes on BP and DP. It was found that the Q_m values of AB25 are higher than those of AG25 on DP (63.3 mg g^{-1}) (Hameed & Hakimi, 2008), AV54 on BP (36.5 mg g^{-1}) (Kumar et al., 2010), and CR on BP (1.7 mg g^{-1}) (Mondal & Kar, 2018). The higher adsorption efficiency of AB25 could be ascribed to its smaller molecular size compared to AG25, AV54, and CR, thus it experiences less steric hindrance to being adsorbed on the surface of the agricultural wastes.

The effect of pH

In real application, the presence of other chemicals could change the pH of wastewater which would potentially affect the adsorption capacity of adsorbent for synthetic dyes. To simulate this
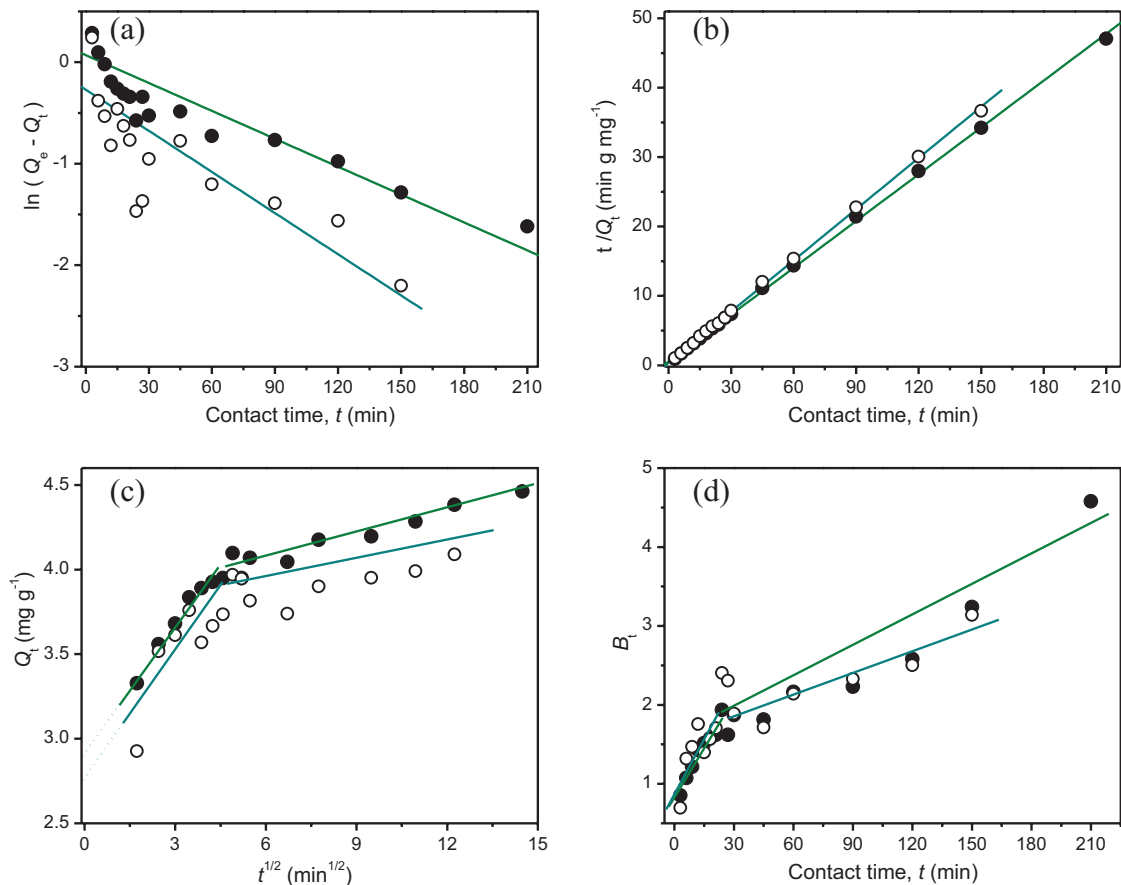
Figure 4. Adsorption kinetic data of 2.40×10^{-4} mol L^{-1} AB25 solutions in the presence of 100 mg of BP (○) and DP (•) simulated with (a) the Lagergren pseudo-first order, (b) pseudo-second order, (c) the Weber–Morris, and (d) the Boyd model.

Table 2. The Adsorption Kinetics Parameters of Lagergren Pseudo-First Order and Pseudo-Second Order Kinetics Models on the Experimental Data of AB25 Adsorption on BP and DP.

KINETICS MODEL	PARAMETERS	BP	DP
Lagergren pseudo-first order	$Q_{e,calc}$ (mg g^{-1})	0.763	1.07
	k_1 (minute^{-1})	0.014	0.009
	R^2	0.519	0.627
Pseudo-second order	$Q_{e,calc}$ (mg g^{-1})	4.07	4.49
	k_2 (g mg^{-1} minute^{-1})	0.163	0.092
	R^2	0.999	0.999

condition, the effect of the pH of the medium on the adsorption of AB25 was evaluated in the range of pH 3 to 10. As shown in Figure 6, at pH 3, the Q_e values of AB25 on BP and DP were 4.69 and 5.03 mg g^{-1}, respectively, and the removal of the acidic synthetic dye decreased gradually with pH. It can be rationalized that, at pH level below pH$_{pzc}$, the functional groups on the adsorbent surface were either protonated or positively charged, while AB25 existed in its anionic form. In this sense, the adsorbent surface facilitated electrostatic and hydrogen bonding interactions. This generated better chemical anchors for the adsorption of AB25. As the medium pH was increased above pH$_{pzc}$, the Q_e

values continued to decrease until it had decreased by approximately 21% at pH > 9. This is most likely due to changes in electronic state of AB25. The relatively small effect of medium pH on the dye removal efficiency suggests that hydrogen bonding was the predominant interaction responsible for the adsorption of AB25 on BP and DP. This is schematically illustrated in Figure 7. A similar adsorption mechanism has also been proposed for the adsorption of AB25 on adsorbents derived from different agricultural wastes, such as cempedak durian peel (Dahri et al., 2016), soybean waste (Kooh et al., 2016), and *Azolla pinnata* (Kooh et al., 2016).
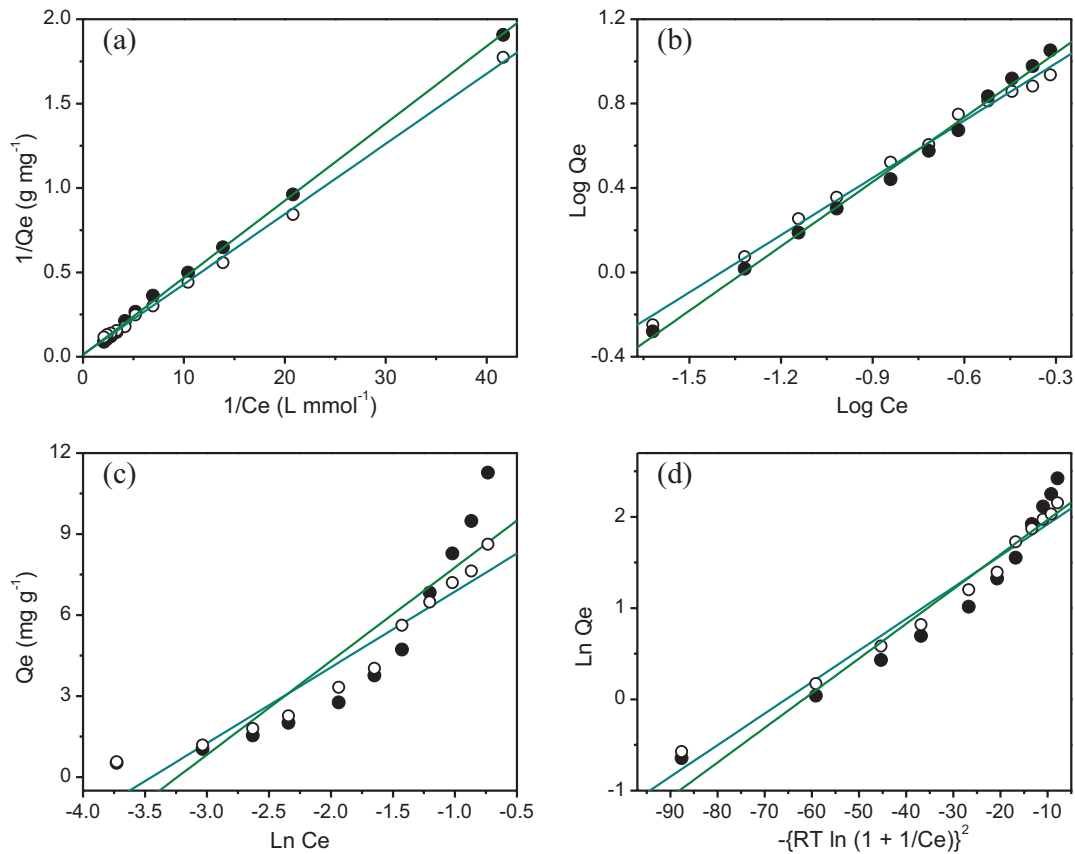
Figure 5. Adsorption isotherm data of AB25 solutions with the initial concentrations of 0.24×10^{-4}–4.80×10^{-4} mol L^{-1} in the presence of 100 mg of BP ($\circ$) and DP ($\bullet$), simulated with: (a) Langmuir, (b) Freundlich, (c) Temkin, and (d) Dubinin-Radushkevich isotherm models. The solid line represents the best fits of the respective isotherm model.

Table 3. The Parameters of Simulation Plots of Various Empirical Isotherm Models With Two Parameters on the Experimental Data.

ISOTHERM MODEL	PARAMETERS	BP	DP
Langmuir	Q_m (mg g^{-1})	70.0	89.7
	K_L (L mmol^{-1})	0.344	0.244
	R^2	0.998	0.999
Freundlich	K_F	18.29	22.15
	n	1.105	0.982
	R^2	0.994	0.995
Temkin	K_T (L mmol^{-1})	31.4	25.5
	b_T (kJ mol^{-1})	0.882	0.714
	R^2	0.924	0.825
Dubinin–Radushkevich	Q_m (mg g^{-1})	9.64	10.5
	β (J mol^{-1})	0.035	0.038
	E (kJ mol^{-1})	3.80	3.78
	R^2	0.978	0.934

## *Thermodynamics of the adsorption of AB25 on BP and DP*

The adsorption of AB25 on BP and DP at different temperatures revealed that the K_L values, and hence K_e^0 values, increased with temperature. This finding implies that the adsorption process was more favorable at higher temperatures. The Gibbs free energy (ΔG_{ads}) was then estimated based on the Van't Hoff equation;

$$\Delta G_{ads} = -RT \ln K_e^0 \tag{11}$$

It was found that ΔG_{ads} values were in the range of –14.66 to –14.74 kJ mol^{-1} and –13.62 to –13.64 kJ mol^{-1} for the adsorption of AB25 on BP and DP, respectively. The negative ΔG_{ads} values confirm that the adsorption process is spontaneous. From the linear plot of ΔG_{ads} values against T, as shown Supplemental Figure S4, the enthalpy (ΔH) values of the adsorption of AB25 on BP and DP were estimated to be –12.1 and –13.4 kJ mol^{-1}, while the entropy (ΔS) values of the adsorption process were found to be 8.02 and 0.82 kJ mol^{-1} K^{-1}, respectively. These thermodynamic parameters show that the adsorption process is exothermic, and that irregularity on the surfaces of the adsorbents increased upon the adsorption of AB25 (Ghosh & Goswami, 2006; Jiménez-ángeles et al., 2017).

Table 4. A Comparison of Q_m Values of Various Types of Adsorbents in the Removal of AB25 From Aqueous Solution.

| ADSORBENT	Q_m (MG G^{-1})	REFERENCE
Shorea dasyphylla sawdust	24.4	Hanafiah et al. (2012)
Pine sawdust	26.2	Ferrero (2007)
Cempedak durian peel	26.6	Dahri et al. (2016)
Oak sawdust	27.9	Ferrero (2007)
Rubber leaf powder	28.1	Khalid et al. (2015)
Rambutan seed	35.6	Lakkaboyana et al. (2018)
Walnut sawdust	37.0	Ferrero (2007)
Soybean waste	38.3	Kooh et al. (2016)
Azolla pinnata	50.5	Kooh et al. (2016)
Hazelnut shell	60.2	Ferrero (2007)
Ficus racemosa leaf powder	83.3	Jain and Gogate (2017)
Modified banana peel in KNO$_3$	89.5	Guiso et al. (2014)
Peach seed powder	95.2	Kul et al. (2019)
Aspergillus oryzae	105.3	Yang et al. (2011)
Egg shell modified activated carbon	109.8	Tovar-Gómez et al. (2012)
Ceratophylum demersum	129.7	Kousha et al. (2014)
Potamogeton pusillus	183.5	Kousha et al. (2014)
Penaeus indicus shell	415.3	Kousha et al. (2015)
Lychee (*Litchi chinensis*) peel	200.0	Bhatnagar and Minocha (2010)
Waste tea activated carbon	203.3	Auta and Hameed (2011)
Pectin derived from pomelo peel	719.4	Shahrin et al. (2021)
Banana peel	70.0	This work
Durian peel	89.7	This work
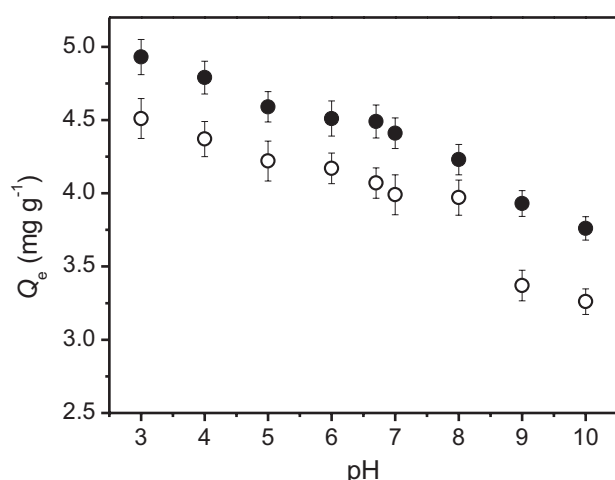
Figure 6. The effect of pH on the adsorption capacity (Q_e) value of 2.40×10^{-4} mol L^{-1} AB25 solutions in the presence of 100 mg of BP (○) and DP (●) after a contact time of 240 minutes.

Regeneration of BP and DP

Desorption of AB25 from the spent BP and DP was achieved by washing them in acidic, basic, and aqueous solutions. The regenerated adsorbents were recycled for the removal of AB25 for a few adsorption-desorption cycles. Figure 8 shows that washing the spent adsorbents with acid was the most effective method to regenerate BP and DP, where the Q_e values of AB25 decreased by less than 25% after the sixth adsorption-desorption cycle. In comparison, washing the spent adsorbents with alkali solution abruptly decreased the Q_e value by 50% after the first cycle, and it continued to gradually decrease after subsequent cycles. Rinsing the spent adsorbents with water resulted in poorer adsorptive performance recovery, as the Q_e value continuously decreased by more than 85% after the sixth cycle. This result indicates that acid treatment efficiently desorbs AB25 from the spent BP and DP and revives the active sites on the adsorbent surfaces. It might be interesting to note
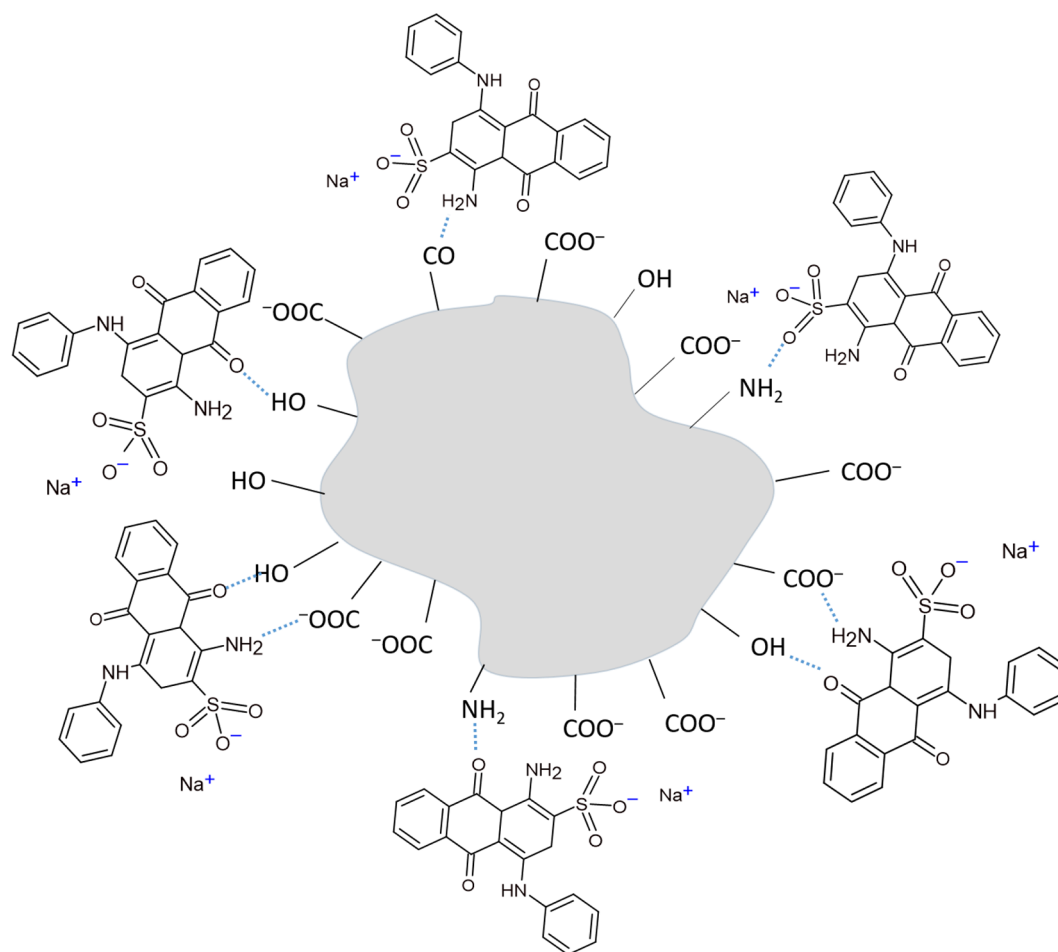
Figure 7. A schematic illustration of the proposed adsorption of AB25 on agricultural wastes.
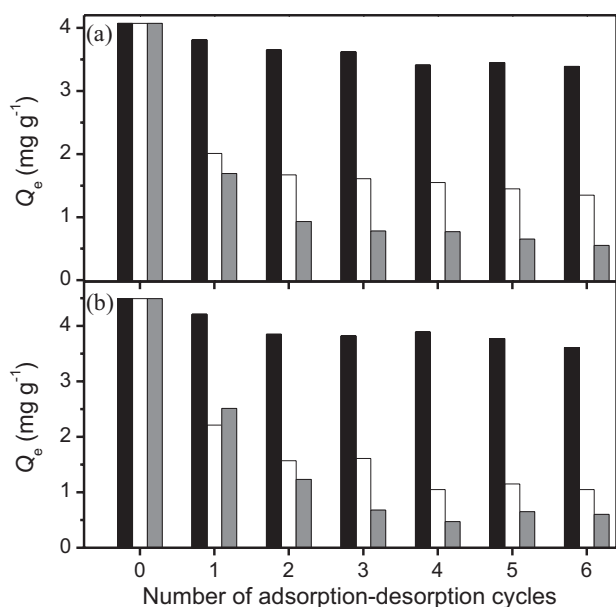
Figure 8. The adsorption capacity (Q_e) value of 2.40×10^{-4} mol L^{-1} AB25 solutions in the presence of: (a) 100 mg of BP and (b) 100 mg of DP regenerated by different desorbing agents; that is, 0.01 M HCl (black bars), 0.01 M NaOH (white bars), and H$_2$O (gray bars), after a contact time of 240 minutes.

that acid treatment has also been revealed to regenerate adsorbents derived from different types of agricultural wastes (Zaidi et al., 2018). We therefore conclude that acid treatment is the most promising method to refresh functional groups on the active sites of agricultural wastes after they have been occupied by synthetic dyes through hydrogen bonding interactions.

Conclusions

The adsorption behavior of Acid Blue 25 (AB25) in an aqueous solution onto banana (BP) and durian (DP) peels has been investigated in batch system using a range of different parameters, including contact time, initial concentration, pH, and temperature. The adsorption of AB25 on the two adsorbents showed similar features, where the kinetics was pseudo-second order and was governed by a two-step intraparticle diffusion, attributed to the external mass transfer pore-volume diffusion. The equilibrium adsorption data were well simulated by the Langmuir isotherm model, suggesting that the adsorption occurred on active sites with homogeneous binding energy on the monolayer surface of both adsorbents. The adsorption process of AB25 on BP and DP was spontaneous and exothermic in nature. Increasing the medium pH decreased the adsorption capacity of the two adsorbents, suggesting that

electrostatic interactions dominated in the adsorption process. The spent BP and DP were successfully regenerated by acid treatment and they could be recycled for the removal of more AB25. The removal efficiency of AB25 on the regenerated adsorbents decreased by less than 25% after the sixth adsorption-desorption cycle, highlighting the key important role of their functional groups in the adsorption of the anionic synthetic dye. Under ambient conditions, the maximum monolayer adsorption capacity (Q_m) values of AB25 on BP and DP were 70.0 and 89.7 mg g^{-1}, respectively. Although the Q_m values of AB25 on BP and DP were slightly higher than those on a large variety of adsorbents derived from agricultural wastes, they were much lower compared to those on activated carbons, polymer-clay nanocomposites, and biopolymers. The results revealed that BP and DP had similar functional groups which generate a negative net charge at ambient pH, and thus they had similar limitations with respect to the removal of acidic synthetic dyes, as represented by AB25, from their aqueous solutions. In order to optimize and improve their adsorptive performance, BP and DP might need further modifications or treatments, for instance, by soaking them in strong acids to remove lignin and other chemicals in order to expose more functional groups with strong hydrogen bonding capabilities on the adsorbent surface as well as to increase the surface area and pore volume.

Credit Author Statement
JHS carried out the adsorption experiments, MAA involved in the sample processing, NAAS, KMP, EK, and AHM contributed in sample characterization, NNMS edited the manuscript, JH analyzed the data, reviewed, and edited the manuscript AU conceptualized, supervised the experiments, interpreted the data, and wrote the manuscript.

Declaration of Conflicting Interests
The author(s) declared no potential conflicts of interest with respect to the research, authorship, and/or publication of this article.

ORCID iD
Anwar Usman https://orcid.org/0000-0002-8199-2931

Supplemental Material
Supplemental material for this article is available online.

REFERENCES
Alshameri, A., Wei, X., Wang, H., Fuguo, Y., Chen, X., He, H., Yan, C., & Xu, F. (2019). A review of the role of natural clay minerals as effective adsorbents and an alternative source of minerals. In K. S. Essa (Ed.), *Minerals* (pp. 49–64). IntechOpen.

Alwi, R. S., Gopinathan, R., Bhowal, A., & Garlapati, C. (2020). Adsorption characteristics of activated carbon for the reclamation of Eosin Y and indigo carmine colored effluents and new isotherm model. *Molecules*, 25, 6014.

Asbollah, M. A., Mahadi, A. H., Kusrini, E., & Usman, A. (2021). Synergistic effect in concurrent removal of toxic methylene blue and acid red-1 dyes from aqueous solution by durian rind: Kinetics, isotherm, thermodynamics, and mechanism. *International Journal of Phytoremediation*, 23, 1432–1443.

Auta, M., & Hameed, B. H. (2011). Preparation of waste tea activated carbon using potassium acetate as an activating agent for adsorption of acid blue 25 dye. *Chemical Engineering Journal*, 171, 502–509.

Bhatnagar, A., & Minocha, A. K. (2010). Assessment of the biosorption characteristics of lychee (litchi chinensis) peel waste for the removal of acid blue 25 dye from water. *Environmental Technology*, 31, 97–105.

Bhatt, R. R., & Shah, B. A. (2015). Sorption studies of heavy metal ions by salicylic acid–formaldehyde–catechol terpolymeric resin: Isotherm, kinetic and thermodynamics. *Arabian Journal of Chemistry*, 8, 414–426.

Boretti, A., & Rosa, L. (2019). Reassessing the projections of the world water development report. *Clean Water*, 2(1), 15.

Chiou, M. S., & Chuang, G. S. (2006). Competitive adsorption of dye metanil yellow and RB15 in acid solutions on chemically cross-linked chitosan beads. *Chemosphere*, 62, 731–740.

Dahri, M. K., Lim, L. B. L., Priyantha, N., & Chan, C. M. (2016). Removal of acid blue 25 using cempedak durian peel from aqueous medium: Isotherm, kinetics and thermodynamics studies. *International Food Research Journal*, 23(3), 1154–1163.

De Gisi, S., Lofrano, G., Grassi, M., & Notarnicola, M. (2016). Characteristics and adsorption capacities of low-cost sorbents for wastewater treatment: A review. *Sustainable Materials and Technologies*, 9, 10–40.

Deshmukh, P. D., Khadse, G. K., Shinde, V. M., & Labhasetwar, P. (2017). Cadmium removal from aqueous solutions using dried banana peels as an adsorbent: Kinetics and equilibrium modeling. *Journal of Bioremediation & Biodegradation*, 8, 395.

Dinh, V.-P., Huynh, T. D., Le, H. M., Nguyen, V.-D., Dao, V.-A., Hung, N. Q., Tuyen, L. A., Lee, S., Yi, J., Nguyen, T. D., & Tan, L. V. (2019). Insight into the adsorption mechanisms of methylene blue and chromium(III) from aqueous solution onto pomelo fruit peel. *RSC Advances*, 9, 25847–25860.

Dotto, G. L., & Pinto, L. A. (2012). Analysis of mass transfer kinetics in the biosorption of synthetic dyes onto Spirulina platensis nanoparticles. *Biochemical Engineering Journal*, 68, 85–90.

El-Hamshary, H., Elsherbiny, A. S., El-Newehy, M. H., & El-Hefnawy, M. E. (2020). Polyaspartate-Ionene/Na+-Montmorillonite nanocomposites as novel adsorbent for anionic dye; effect of ionene structure. *Polymers*, 12, 2843.

El-Khaiary, M. I., & Malash, G. F. (2011). Common data analysis errors in batch adsorption studies. *Hydrometallurgy*, 105, 314–320.

Ferrero, F. (2007). Dye removal by low cost adsorbents: Hazelnut shells in comparison with wood sawdust. *Journal of Hazardous Materials*, 142, 144–152.

Fierro, V., Torné-Fernández, V., Montané, D., & Celzard, A. (2008). Adsorption of phenol onto activated carbons having different textural and surface properties. *Microporous and Mesoporous Materials*, 111, 276–284.

Ghaffari, H. R., Pasalari, H., Tajvar, A. H., Dindarloo, K., Goudarzi, B., Alipour, V., & Ghanbarneajd, A. (2017). Linear and nonlinear two-parameter adsorption isotherm modeling: A case-study. *International Journal of Engineering Science*, 6(9), 1–11.

Ghosh, U. C., & Goswami, S. (2006). Studies on adsorption behaviour of Cr(VI) onto synthetic hydrous stannic oxide. *Water SA*, 31, 597–602.

Guiso, M. G., Biesuz, R., Vilariño, T., López-García, M., Rodríguez Barro, P., & Sastre de Vicente, M. E. (2014). Adsorption of the prototype anionic anthraquinone, acid blue 25, on a modified banana peel: Comparison with equilibrium and kinetic ligand–receptor biochemical data. *Industrial & Engineering Chemistry Research*, 53, 2251–2260.

Hameed, B. H., & Hakimi, H. (2008). Utilization of durian (Durio zibethinus Murray) peel as low cost sorbent for the removal of acid dye from aqueous solutions. *Biochemical Engineering Journal*, 39, 338–343.

Hanafiah, M. A. K. M., Ngah, W. S. W., Zolkafly, S. H., Teong, L. C., & Majid, Z. A. A. (2012). Acid blue 25 adsorption on base treated Shorea dasyphylla sawdust: Kinetic, isotherm, thermodynamic and spectroscopic analysis. *Journal of Environmental Sciences*, 24(2), 261–268.

Ho, Y. S., Ng, J. C., & McKay, G. (2000). Kinetics of pollutant sorption by biosorbents: Review. *Separation and Purification Methods*, 29, 189–232.

Hubbe, M., Azizian, S., & Douven, S. (2019). Implications of apparent pseudo-second-order adsorption kinetics onto cellulosic materials: A review. *BioResources*, 14, 7582–7626.

Jain, S. N., & Gogate, P. R. (2017). NaOH-treated dead leaves of ficus racemosa as an efficient biosorbent for acid blue 25 removal. *International Journal of Environmental Science and Technology*, 14, 531–542.

Jawad, A. H., Rashid, R. A., Ishak, M. A. M., & Ismail, K. (2018). Adsorptive removal of methylene blue by chemically treated cellulosic waste banana (*Musa sapientum*) peels. *Journal of Taibah University for Science*, 12(6), 809–819.

Jiménez-ángeles, F., Khoshnood, A., & Firoozabadi, A. (2017). Molecular dynamics simulation of the adsorption and aggregation of ionic surfactants at liquid–solid interfaces. *The Journal of Physical Chemistry B*, 121, 25908–25920.

Khalid, K., Ngah, W. S. W., Hanafiah, M. A. K. M., Malek, N. S. A., & Khazaai, S. N. M. (2015). Acid blue 25 adsorption onto phosphoric acid treated rubber leaf powder. *American Journal of Environmental Engineering*, 5, 19–25.

Kooh, M. R. R., Dahri, M. K., Lim, L. B. L., & Lim, L. H. (2016). Batch adsorption studies on the removal of acid blue 25 from aqueous solution using Azolla pinnata and soya bean waste. *Arabian Journal for Science and Engineering*, 41, 2453–2464.

Kousha, M., Daneshvar, E., Esmaeili, A. R., Zilouei, H., & Karimi, K. (2014). Biosorption of toxic acidic dye–acid blue 25, by aquatic plants. *Desalination and Water Treatment*, 52, 6756–6769.

Kousha, M., Tavakoli, S., Daneshvar, E., Vazirzadeh, A., & Bhatnagar, A. (2015). Central composite design optimization of acid blue 25 dye biosorption using shrimp shell biomass. *Journal of Molecular Liquids*, 207, 266–273.

Kul, A. R., Aldemir, A., & Elik, H. (2019). Adsorption of acid blue 25 on peach seed powder: Isotherm, kinetic and thermodynamic studies. *Environmental Research and Technology*, 2(4), 233–242.

Kumar, G. V., Ramalingam, P., Kim, M. J., Yoo, C. K., & Kumar, M. D. (2010). Removal of acid dye (violet 54) and adsorption kinetics model of using musa spp. Waste: A low-cost natural sorbent material. *Korean Journal of Chemical Engineering*, 27, 1469–1475.

Lakkaboyana, S. K., Khantong, S., Kabir, M. A., Ali, Y., & Yaacob, W. Z. W. (2018). Removal of acid blue 25 dye from wastewater using rambutan (*Nephelium lappaceum* Linn.) seed as an efficient natural biosorbent. *Indian Journal of Advanced Chemical Sciences*, 6, 111–117.

Lewis, D. M. (2009). The coloration of wool. In Johnson, N. A. G., & Russell, I. M. (Eds.), *Advances in wool technology* (pp. 183–213). Woodhead Publishing Limited.

Lima, E. C., Hosseini-Bandegharaei, A., Moreno-Piraján, J. C., & Anastopoulos, I. (2019). A critical review of the estimation of the thermodynamic parameters on adsorption equilibria. Wrong use of equilibrium constant in the Van't hoof equation for calculation of thermodynamic parameters of adsorption. *Journal of Molecular Liquids*, 273, 425–434.

Mohammed, S. A., Najib, N. W. A. Z., & Muniandi, V. (2012). Durian rind as a low cost adsorbent. *International Journal of Civil and Environmental Engineering*, 12, 51–56.

Mondal, N. K., & Kar, S. (2018). Potentiality of banana peel for removal of Congo red dye from aqueous solution: Isotherm, kinetics and thermodynamics studies. *Applied Water Science*, 8, 157.

Palani, G., Arputhalatha, A., Kannan, K., Lakkaboyana, S. K., Hanafiah, M. M., Kumar, V., & Marella, R. K. (2021). Current trends in the application of nanomaterials for the removal of pollutants from industrial wastewater Treatment-A review. *Molecules*, 26, 2799.

Pathak, P. D., Mandavgane, S. A., & Kulkarni, B. D. (2017). Fruit peel waste:characterization and its potential uses. *Current Science*, 113, 444–454.

Payus, C. M., Refdin, M. A., Zahari, N. Z., Rimba, A. B., Geetha, M., Saroj, C., Gasparatos, A., Fukushi, K., & Alvin Oliver, P. (2021). Durian husk wastes as low-cost adsorbent for physical pollutants removal: Groundwater supply. *Materials Today Proceedings*, 42, 80–87.

Piaskowski, K., Świderska-Dąbrowska, R., & Zarzycki, P. K. (2018). Dye removal from water and wastewater using various physical, chemical, and biological processes. *Journal of AOAC International*, 101, 1371–1384.

Rafatullah, M., Sulaiman, O., Hashim, R., & Ahmad, A. (2010). Adsorption of methylene blue on low-cost adsorbents: A review. *Journal of Hazardous Materials*, 177, 70–80.

Robati, D. (2013). Pseudo-second-order kinetic equations for modeling adsorption systems for removal of lead ions using multi-walled carbon nanotube. *Journal of Nanostructure in Chemistry*, 3, 55.

Shahrin, E. W. E., Narudin, N. A. H., Padmosoedarso, K. M., Kusrini, E., Mahadi, A. H., Shahri, N. N. M., & Usman, A. (2021). Pectin derived from pomelo pith as a superior adsorbent to remove toxic acid blue 25 from aqueous solution. *Carbohydrate Polymer Technologies and Applications*, 2, 100116.

Sharma, P., & Das, M. R. (2013). Removal of a cationic dye from aqueous solution using graphene oxide nanosheets: Investigation of adsorption parameters. *Journal of Chemical and Engineering Data*, 58, 151–158.

Simonin, J. P. (2016). On the comparison of pseudo-first order and pseudo-second order rate laws in the modeling of adsorption kinetics. *Chemical Engineering Journal*, 300, 254–263.

Srivatsav, P., Bhargav, B. S., Shanmugasundaram, V., Arun, J., Gopinath, K. P., & Bhatnagar, A. (2020). Biochar as an eco-friendly and economical adsorbent for the removal of colorants (dyes) from aqueous environment: A review. *Water*, 12, 3561.

Tovar-Gómez, R., Rivera-Ramírez, D. A., Hernández-Montoya, V., Bonilla-Petriciolet, A., Durán-Valle, C. J., & Montes-Morán, M. A. (2012). Synergic adsorption in the simultaneous removal of acid blue 25 and heavy metals from water using a Ca(PO3)2-modified carbon. *Journal of Hazardous Materials*, 199–200, 290–300.

Viegas, R. M. C., Campinas, M., Costa, H., & Rosa, M. J. (2014). How do the HSDM and Boyd's model compare for estimating intraparticle diffusion coefficients in adsorption processes. *Adsorption*, 20, 737–746.

Yang, Y., Jin, D., Wang, G., Wang, S., Jia, X., & Zhao, Y. (2011). Competitive biosorption of acid blue 25 and acid Red 337 onto unmodified and CDAB-modified biomass of Aspergillus oryzae. *Bioresource Technology*, 102, 7429–7436.

Zaidi, N. A. H. M., Lim, L. B. L., Priyantha, N., & Usman, A. (2018). Artocarpus odoratissimus leaves as an eco-friendly adsorbent for the removal of toxic rhodamine B dye in aqueous solution: Equilibrium isotherm, kinetics, thermodynamics and regeneration studies. *Arabian Journal for Science and Engineering*, 43, 6011–6020.

Zaidi, N. A. H. M., Lim, L. B. L., & Usman, A. (2019). Enhancing adsorption of malachite green dye using base-modified Artocarpus odoratissimus leaves as adsorbents. *Environmental Technology & Innovation*, 13, 211–223.

Zamri, N. I. I., Zulmajdi, S. L. N., Daud, N. Z. A., Mahadi, A. H., Kusrini, E., & Usman, A. (2021). Insight into the adsorption kinetics, mechanism, and thermodynamics of methylene blue from aqueous solution onto pectin-alginate-titania composite microparticles. *SN Applied Science*, 3, 222.

Zeng, Y., Chen, X., Zhao, D., Li, H., Zhang, Y., & Xiao, X. (2012). Estimation of pKa values for carboxylic acids, alcohols, phenols and amines using changes in the relative gibbs free energy. *Fluid Phase Equilibria*, 313, 148–155.